Advanced Robotics

ISSN: 0169-1864 (Print) 1568-5535 (Online) Journal homepage: http://www.tandfonline.com/loi/tadr20

Key design parameters of a few types of electro-hydrostatic actuators for humanoid robots

Tianyi Ko, Hiroshi Kaminaga & Yoshihiko Nakamura

To cite this article: Tianyi Ko, Hiroshi Kaminaga & Yoshihiko Nakamura (2018): Key design parameters of a few types of electro-hydrostatic actuators for humanoid robots, Advanced Robotics, DOI: 10.1080/01691864.2018.1545604

To link to this article: https://doi.org/10.1080/01691864.2018.1545604

Published online: 14 Nov 2018.

Submit your article to this journal

Article views: 4

View Crossmark data

Full Terms & Conditions of access and use can be found at
http://www.tandfonline.com/action/journalInformation?journalCode=tadr20

ADVANCED ROBOTICS
https://doi.org/10.1080/01691864.2018.1545604

FULL PAPER

Key design parameters of a few types of electro-hydrostatic actuators for humanoid robots

Tianyi Ko, Hiroshi Kaminaga and Yoshihiko Nakamura

Department of Mechano-Informatics, Graduate School of Information Science and Technology, The University of Tokyo, Tokyo, Japan

ABSTRACT

To overcome the tradeoff between the bandwidth and force-to-weight ratio of the backdrivable actuators, actuation by electro-hydrostatic actuators (EHA) is effective. Based on the idea, we developed the adult size, humanoid robot 'Hydra', whose joints are driven by EHA. In its development, a critical problem was the insufficient force of the available lightweight and backdrivable EHA. In this paper, we present our approach to enhance their maximum force while keeping them small, lightweight and backdrivable. We first analyze the behavior of EHA and show that the maximum force is enabled on the balance between the viscous loss and the internal leakage loss. We also show that miniaturization of the actuator moves the system to the internal leakage loss dominant side, and to encounter this, reduction of the internal gap, maintain of the fluid viscosity, and full utilization of the space to enlarge the pressure receiving surface are effective. The mechanical design process and experimental evaluation on each of these three aspects are detailed.

ARTICLE HISTORY
Received 28 February 2018
Revised 10 August 2018
Accepted 15 October 2018

KEYWORDS
Actuator; EHA; hydraulic; force control; backdrivability

1. Introduction

For the next generation of robots which try to move from well-defined environments such as factories or labs to unstructured environments closer to or extremely far from our lives, backdrivability of the actuators has been an important requirement. While actuation by the servo-valve controlled hydraulic systems or the combination of an electric motor and high reduction-ratio gear-train have high performance on the response and force-to-weight ratio, their backdrivability is limited by the large friction in the force transmission. To improve the backdrivability of robot actuators, many approaches have been taken.

Asada et al. [1] developed a direct-drive robot arm with electric motors inside the joints. Wensing et al. [2] realized fast and compliant actuation by a combination of small reduction-ratio gear and large torque motor. While the direct-drive or low reduction-ratio geared systems have high control bandwidth and backdrivability, they are limited in torque density. Insertion of series elasticity to a low-backdrivability actuator is a natural approach considering the model of muscles by Hill [3]. Hyodo et al. [4] developed an antagonistically tendon driven joint with non-linear series elasticity. Pratt et al. [5] developed a series elastic actuator for legged robots. Recent outstanding works as a system includes WALK-MAN by Tsagarakis et al. [6], CHIMP by Stentz et al. [7], and THOR by Knabe et al. [8]. They also expanded to variable stiffness actuators, such as the work by Grebenstein et al. [9]. The difficulty of series elastic actuators is on the control side, due to the delay originated in the elasticity and the oscillating nature. Pneumatic actuators have the similar property of high backdrivability but low bandwidth [10]. The representing works include the work by Caldwell et al. [11], LUCY by Verrelst et al. [12] and the athlete robot by Niiyama et al. [13].

To enable a backdrivable robot joint without explicit series elasticity, we have been proposing the actuation by electro-hydrostatic actuators (EHA). In EHA, the speed reduction and force magnifying are done by the difference of the pressure receiving surface of the input and output side, based on the principle of Pascal. Thanks to the removal of the gear transmissions, EHAs can be designed to have high backdrivability [14]. They also have high energy efficiency than the servo-valve controlled hydraulic systems, since they can generate the necessary pressure on demand or store the pressure in an accumulator [15].

The humanoid robot 'Hydra' [16] (Figure 1) is an adult size humanoid robot whose 40 joints are driven by

CONTACT Tianyi Ko kang@ynl.t.u-tokyo.ac.jp Department of Mechano-Informatics, Graduate School of Information Science and Technology, The University of Tokyo, 7-3-1 Hongo, Bunkyo-Ku, Tokyo, Japan
This paper is selected as the 'Cutting Edge of Robotics in Japan' by the Editorial Committee of Advanced Robotics.

© 2018 Informa UK Limited, trading as Taylor & Francis Group and The Robotics Society of Japan

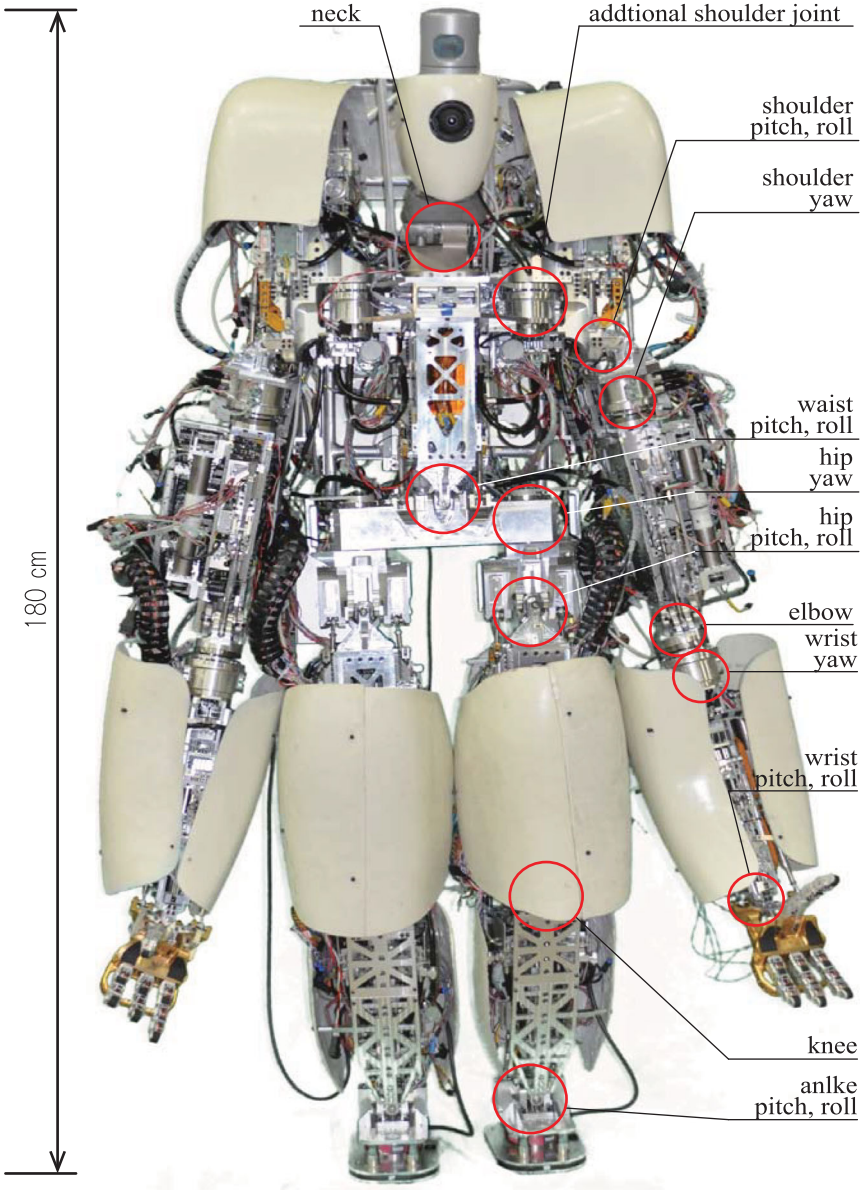

Figure 1. Whole body picture of the humanoid robot Hydra. The outer cover is designed by Prof. Satoru Kitagou, Tokyo University of the Arts.

EHA. In the development of Hydra, a critical problem was their maximum force. While EHA's backdrivability was well studied in the previous works [17], limited attention was paid to their large-force property, or the force-to-weight ratio. The existing lightweight and backdrivable EHAs were not possible to exert enough joint torque to support the whole-body weight, or in the case of the hand, not enough grasping force for heavy tasks. In this paper, we present our approaches to enhance the actuator force while still keeping them lightweight and backdrivable, with which we could create Hydra. Some of the approaches were originally developed independently and heuristically. In this paper, we re-organize them by extracting their common background, which is to reduce the internal leakage. This is necessary because we found that the miniaturization of the system leads the internal leakage to be a dominant source of energy loss, even when other conditions such as the internal gap, fluid viscosity, and total reduction ratio are the same. In Section 2, we analyze the factors that affect the force-to-weight ratio and discuss approaches to improve it, showing the scale effect on the torque density of EHA. This leads the requirement that when an EHA is to be miniaturized, it is necessary to reduce the internal gap, maintain the fluid viscosity, and maximize the effective pressure receiving surface under the outer size constraint. In Section 3, we show the way to keep the internal gap small, from both the pump and the actuator side. In Section 4, we present the direct water cooling of the pump to maintain the fluid viscosity. In Section 5, mainly targeting the cluster

actuator for the hand, we show a design that maximally utilizes the space, which actually improves the output force of the actuator. Section 6 concludes the paper.

2. Effect of the internal gap, fluid viscosity and piston bore

When constructing a robot system, many parameters need to be decided at the beginning, such as joint torque, joint maximum velocity, and specification of the electric motors. For the transmission, the total reduction ratio and the torque capacity is decided in the initial requirement definition. In the case of EHA, after the torque capacity and the reduction ratio are given, there are still internal parameters to decide, such as the internal gap of the pump, fluid viscosity, and pressure receiving surface. In this section, we clarify the parameters that are needed to be decided and their effect on the behavior of the hydrostatic transmission.

We first consider the model shown in Figure 2. In the figure, the pump is modeled as a cylinder with a radius of r [m], thickness T [m]. The pump receives an external force/torque input of τ_p [N]. The velocity of the pump is $\dot{\theta}_p$ [m/s] and it discharges the fluid with pressure p [Pa] in the flow rate of Q_q [m^3/s]. Internal leakage is a leak of fluid from the high-pressure side to the low-pressure side in a hydraulic system. In the following, we treat the actuator as a linear cylinder, which has almost zero internal leakage due to the piston seal, therefore we only consider the leak inside the pump. When the Reynolds number is low, the flow of the internal leakage is laminar. In that case, the flow is the Couette–Poiseuille flow, which is a linear sum of the Couette flow and the Poiseuille flow. The former is the drag flow between two surfaces moving tangentially, and the latter is the pressure-induced flow through a channel. The flow velocity distribution in the gap is expressed as

$$u(y) = \frac{\dot{\theta}_p}{h} y + \frac{p}{2\mu(t)T}(y^2 - hy) \tag{1}$$

where $\mu(t)$ [Pa s] is the fluid viscosity and h [m] is the internal gap between the moving part (piston) and the casing (cylinder). The fluid viscosity highly depends on the fluid temperature t [°C]. In our case, the viscosity varies from 0.092 [Pa s] at 40°C to 0.012 [Pa s] at 100°C. The actual discharging flow rate of the pump Q_q [m^3/s] and the pump input force τ_p can be expressed as follows:

$$Q_q = k_p\dot{\theta}_p + \pi hr^2\dot{\theta}_p - \frac{\pi rh^2}{6\mu(t)T}p \tag{2}$$

$$\tau_p = \pi r^2 p + \frac{2\pi\mu(t)rT}{h}\dot{\theta}_p + \frac{\pi hr}{\mu(t)}p \tag{3}$$

where r [m] and T [m] is the radius and thickness of the pump's piston, respectively. In Equation (2), the first term is the theoretical flow. The second term is the drag flow (the Couette flow corresponding to the first term of Equation (1)) and the last term is the internal leakage (the Poiseuille flow corresponding to the second term of Equation (1)). Similarly, in Equation (3), the second term is the viscous friction by the drag flow and the third term is the drag by the internal leakage flow.

From the model, we can see three design parameters that affect the performance: the pump internal gap h, the fluid viscosity μ, and the pressure receiving surface k_q or r.[1] To see their effect, we conducted a series of simulations with a fixed cylinder force (1500 N), velocity

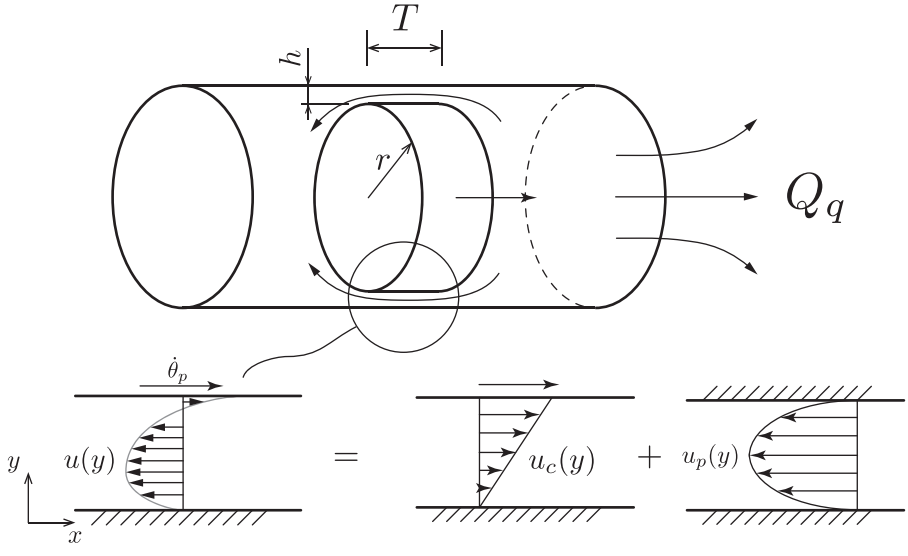

Figure 2. Schematic of a pump with internal leakage.

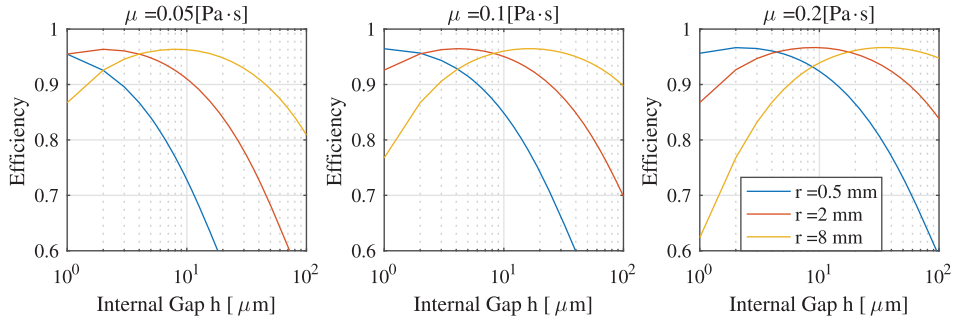

Figure 3. Simulated energy efficiency of an EHA when the piston force, velocity and the total reduction ratio are fixed, while the internal gap, pressure receiving surface, and fluid viscosity vary. The graph suggests that smaller pressure receiving surface has the same effect of a larger internal gap or lower fluid viscosity.

(10 mm/s), and reduction ratio (30), and different variation of h, μ, r. From Equations (2), (3), we get the pump input force and velocity and therefore efficiency, which is plotted in Figure 3. The graph suggests that there is an optimal point, on the balance between viscous loss and internal leakage loss. While it is a matter of course that lower viscosity or larger internal gap results in smaller viscous friction and large internal leakage, it is worth to notice that smaller size also has the same effect. This tells us that minimization of the internal leakage is the key to achieve high force-to-size ratio. We need to reduce the internal gap, maintain the fluid viscosity, and maximize the pressure receiving surface in the limited space, which are detailed in the following subsections.

3. Internal gap control of EHA

3.1. Gap control of pumps by a high stiffness design

Minimization of the pump's internal gap plays an important role to improve the force-to-size ratio of an EHA. In the case of gear pumps, the key is how to reduce the distance between the pump casing and the gears. In our previous work, we saw an unexpectedly large internal leakage and therefore we could not attain the required force. The actuator was an integrated miniature cluster EHA to drive robot hands [18]. We hypothesized that the unexpected large internal gap is because of the mechanical deformation of the pump components. To confirm this, we developed a reinforced version of the pump. The new pump has the same gear as the initial version (The thickness of the gear is doubled, to keep the same reduction ratio when combined with a larger cylinder described later. Their outlook is shown in Figure 12.) Figure 4 shows the cut model of the initial and the modified pump. Their basic structures are the same: the pumps are internal gear pumps with a crescent separator and the pump shafts are driven by an external electric motor. The pump shaft and the inner rotor is supported by ball

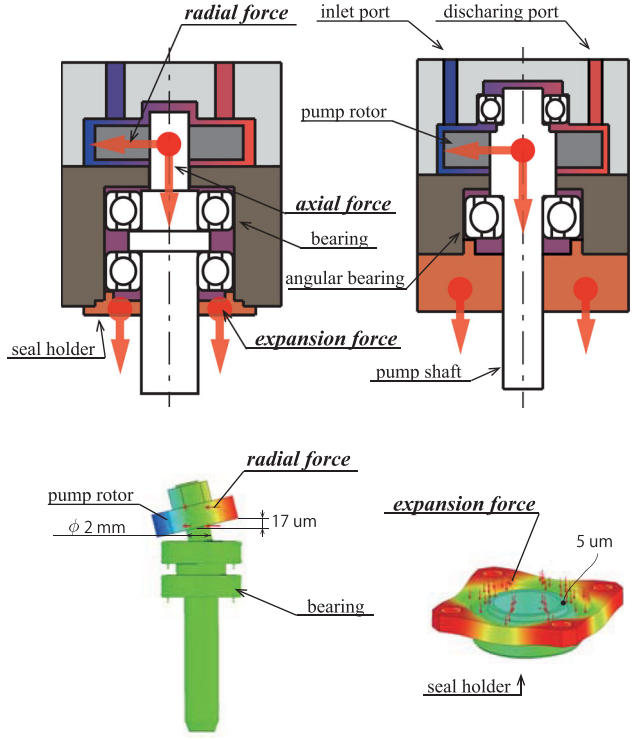

Figure 4. Three forces due to the pressure cause deformation and unexpected internal leakage. The radial force on the pump rotor due to the differential force, the axial force on the pump rotor due to the mean internal pressure, and the expansion force on the pump casing is handled with higher stiffness in the modified design.

bearings. The outer rotor is not shown in the figures. The inlet/discharging ports are placed on the opposite side of the pump shaft.

When the pump generates pressure, there are three major forces that result in the deformation. They are shown in red arrows in the figure. Firstly, the radial force is applied to the pump rotor, since the rotor separates the high-pressure fluid and low-pressure one inside the pump. As shown in the cut model, in the initial pump the rotor is single supported by the bearings. The

deformation of the bearings and the pump shaft results in the unexpected large inner gap. In the left bottom of Figure 4, we show the result of a FEM analysis of the initial pump. In this simulation, the bearings were treated as rigid bodies and only the deformation of the shaft was regarded. With a 5 MPa differential pressure, the rotor tilted with the maximum axial displacement 17 μ m, which happened in the tip of the rotor. One of the reasons causing the large deformation is the thin rod diameter – 2 mm. In the reinforced version, the rotor is modified to be double supported. This is effective because the displacement relies on the square of the distance from the supporting point. The second force is the axial force on the rotor. Since only one side of the pump shaft is exposed to the atmosphere, the force which is the product of the internal mean pressure and the shaft's cross-section tries to push the shaft out of the pump. This is supported by the axial stiffness of the bearings. To have higher axial stiffness, the initial deep groove bearing is replaced by a larger angular bearing. When the internal pressure is 5 MPa, the axial displacement of the rotor is estimated to be suppressed from the original 7.5 to 2.5 μ m, based on the catalog of the bearings [19]. The third force is the expansion force on the pump casing due to the internal mean pressure. In the right bottom of Figure 4, a FEM analysis of the casing is shown. With 5 MPa internal pressure, the deformation is estimated to cause 5 μ m axial displacement of the rotor. The modified pump has a thicker structure with FEM deformation analysis.

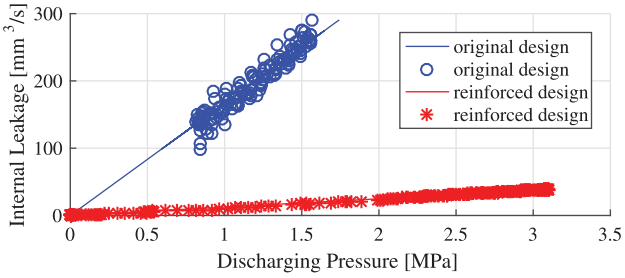

Figure 5. Comparison of the internal leakage of the initial and modified pump. The *y*-axis represents the leakage and the *x*-axis represents the pressure. The experiment was done with the discharging port of the pump closed. The leak is calculated from the rotor speed and the geometric parameters of the pump. The pressure is acquired from the attached pressure sensor. To prevent the heat effect on the amount of leak, the experiment was done in a short time. This graph shows that the new pump has more than 92% less leak for the same pressure.

Figure 5 shows the internal leakage evaluation of the initial and modified pump. The evaluation was done under a condition that the discharging port of the pump was closed. In that case, the amount of the internal leakage equals to the theoretical displacement of the pump, so that we could acquire the value from the pump's geometric specification and the rotational speed. In the graph, the horizontal axis represents the pump pressure and the vertical axis represents the amount of the internal leakage. The comparison shows that the modified pump has more than 92% less internal leakage than the initial version. From the evaluation here, we can say that the effect of the pump's deformation due to the pressure consists a large part of the effective internal gap, and an extra consideration should be taken in the design process.

3.2. Gap control of actuators

3.2.1. Low-friction double rod cylinder with a beam structure

Gap control in the actuator side is also important to improve the force-to-weight ratio of EHA. In the sense of internal leakage reduction, cylinders are advantageous

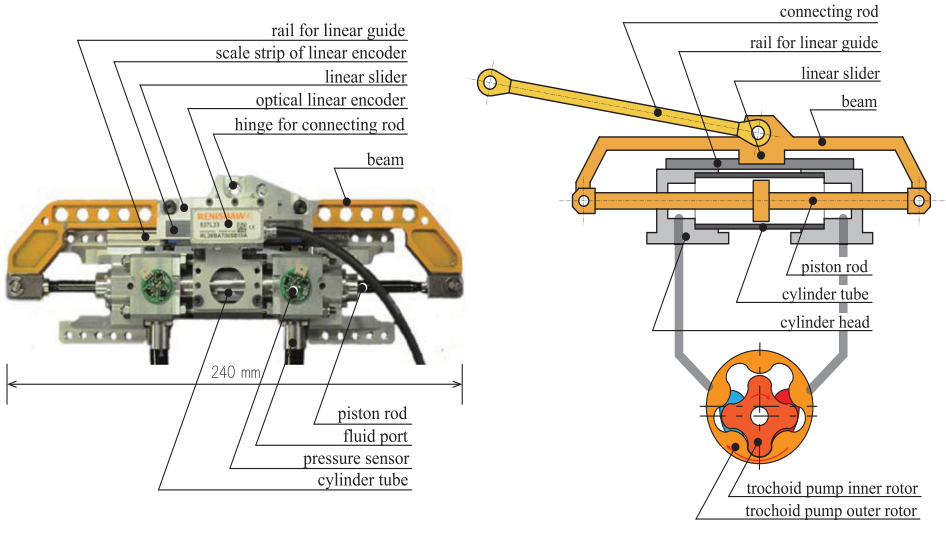

Figure 6. Low friction double-rod cylinder with the beam structure.

Table 1. Specification of the developed double rod cylinder with beam structure. The maximum force and velocity shows the case with the pump described in Section 4.

Weight	600 g
Inner bore	20 mm
Piston rod diameter	6 mm
Full stroke	50 mm
Maximum force	1500 N
Maximum speed	200 mm/s

since it is easy to install piston rings to completely avoid the internal leakage around the piston. Based on this idea, we developed a lightweight cylinder shown in Figure 6. The cylinder has 600 g weight, 240 mm length, 20 mm cylinder bore, and 50 mm stroke. With its 6 mm diameter piston rod, it converts the 5.3 MPa pump pressure to 1500 N piston force. Table 1 summarizes its specification.

To improve the backdrivability, a special friction reduction effort needs to be paid on the actuator. We selected double rod cylinders instead of single rod ones, since the combination of a single rod cylinder and closed hydraulic circuit needs a valve system to compensate the chamber volume change, which results in high viscous friction coming from the small area inside the valve. Figure 7 shows the comparison of an EHA hydraulic circuit with a single rod cylinder and double rod one. The difficulty for double rod cylinders is their high mechanical friction due to the oil seal for the piston rod.

To reduce the rod seal friction, we introduced a beam structure with which the necessary diameter of the piston rod is reduced, therefore the friction on the rod seal could be reduced.

Figure 6 illustrates the idea. In common hydraulic cylinders, the piston rod diameter is decided by the buckling strength. In our design, both ends of the piston rod are held by a beam structure, while the external load is applied on the beam side, rather than the piston rod directly. The beam is held by a linear guide and only transfer the axial force to the piston rod. This removes the possibility of buckling and we can minimize the rod diameter as small as that the tensile strength of one rod is the half of the designed maximum force, since we can now use both of the piston rods to transfer the force.

Another advantage of this structure is that thanks to the linear guide, we can fix the cylinder body on the link when the other end of the connecting rod is attached on a rotational joint. In the common type of rotational joints driven by cylinders, the cylinder needs to swing according to the joint angle. In our fixed cylinder arrangement, in addition to that we can save the space for the swinging, we can minimize the distance between the pump and cylinder with short and stiff piping. This is advantageous in the enhancement of its response.

To see the low-friction performance of the developed cylinder, we conducted a force control experiment. The actuator was under a low-gain position control and the piston is manually moved. The plot between the piston displacement and the measured piston force by an external strain-gauge based sensor is shown in Figure 8. The actuator was controlled to behave as a soft linear spring, therefore the ideal relationship between the displacement and force should be a straight line, as shown in the red line in the figure. The actually measured force, shown in blue markers, had a hysteresis of around 12.1 N RMS error from the ideal line. This is because of the friction on the piston rod oil seal, since the pressure sensor based force measurement for the force controller cannot measure the friction on the oil seal. However, the value is 0.81% of the maximum output force of 1500 N, which proved the low-friction property of the proposed beam structure. While whether this value is acceptable or not is dependent on the application, for a torque-controlled joint, it is a low value since a large number of load-cells have 1%R.O. nonlinearity.

3.2.2. High casing stiffness vane motor

While linear cylinders are advantageous in the reduction of the internal leakage, they are difficult to be applied for joints whose axis is parallel to the longitudinal direction of the link. In such a case, rotary vane motors are a solution, while they are costly in the sense of the complex structure, heavy weight, and limited efficiency/torque due to the internal leakage. To overcome the problem, we took a unique structure shown in Figure 9. In the developed vane motor, the expansion force due to the internal pressure, applied on the casing, is supported by a pair of thrust bearings held by the output shaft. Thanks to this support, the strength of the pump casing can be reduced to save the total weight, while keeping the constant small gap between the vane and the casing. Table 2 summarize the specification. It has 780 g weight and 120° range of motion. The vane converts 5.3 MPa pump pressure to a 60 Nm torque.

4. Fluid viscosity control by direct water cooling of the pump

High fluid viscosity is preferable to minimize the actuator size or relax the internal gap requirement. The problem is that the fluid viscosity becomes smaller when the fluid temperature gets higher. The energy loss due to the friction or internal leakage is converted to the heat. When the transmission is already in the 'too much internal leakage' side from the optimal condition, it results in a positive feedback: energy loss causes higher fluid temperature,

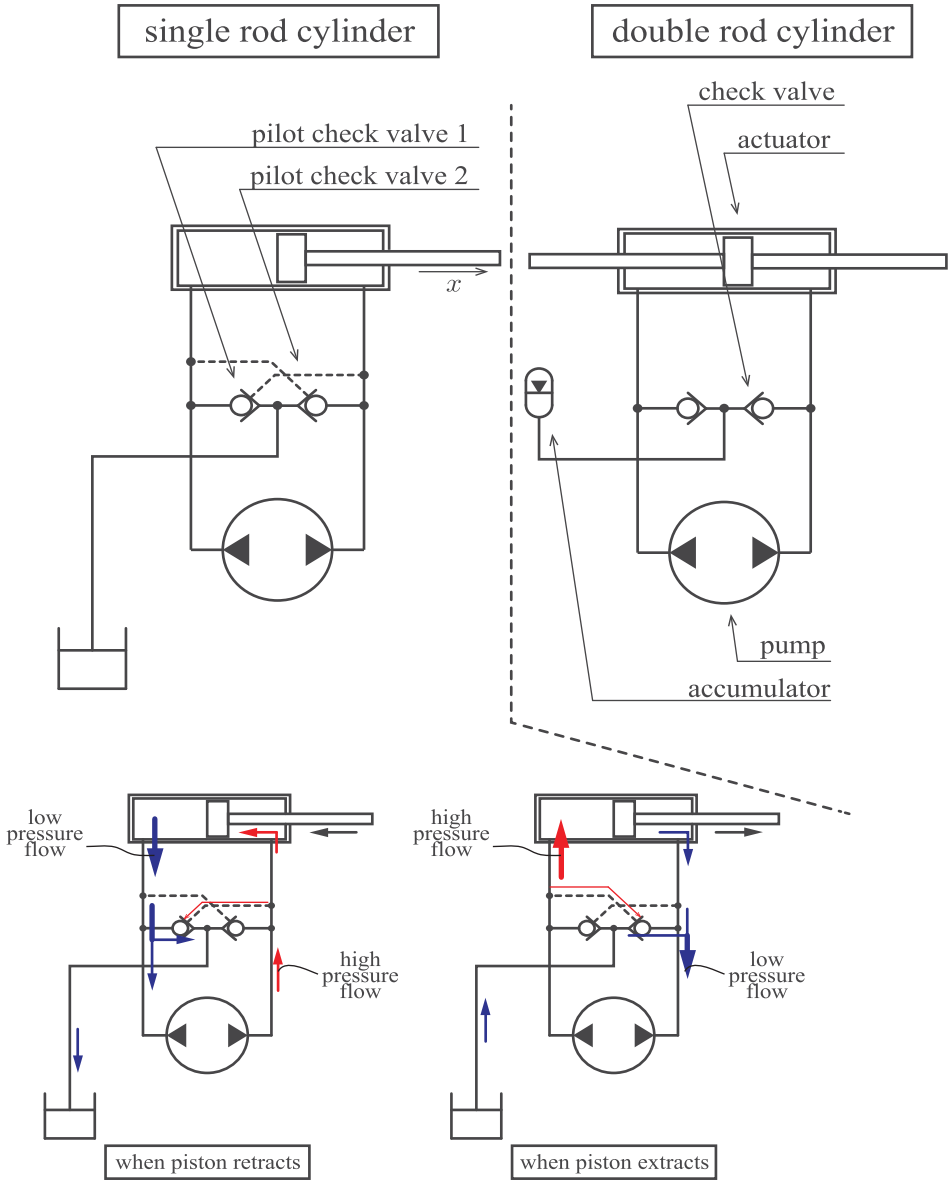

Figure 7. Comparison of an EHA hydraulic circuit with a single rod cylinder (left) and with a symmetric double rod cylinder (right). In the case of double-rod cylinders, only a small capacity accumulator and simple check valves are needed since they work only to compensate the small amount of external leakage and avoid cavitation. In the case of single rod cylinders for closed circuits, the accumulator need to have at least larger capacity than the volume of the piston rod. The check valves need to be pilot check valves. When the cylinder retracts, a larger volume of the fluid moves out from the cylinder than the volume moves in. The differential volume need to be stored in the accumulator through the force cracked pilot check valve. When the cylinder extends, more fluid need to be sent to the cylinder than the fluid moves out. The differential volume is supplied from the accumulator. While in such case the check valve does not necessary to be a pilot one, a pilot check valve is advantageous in smooth operation and avoidance of cavitation.

then less viscosity and less efficiency, therefore even more energy loss. An effective cooling of the fluid is crucial to avoid the decrease of performance. The problem is that unlike the servo valve hydraulics with the open hydraulic circuit, the closed and independent circuit of an EHA is difficult to cool the fluid by commonly used oil coolers. Since the heat is mostly generated in the pump, we take a straightforward approach: directly water cool the pump by introducing a 3D printed coolant channel into the pump casing. Figure 10 illustrates the implementation of the cooling mechanism.

The cooling performance depends on the coolant flow rate and system temperature. In the robot, the coolant circuit is a closed loop with a radiator, therefore it also depends on the atmosphere temperature. To simulate the cooling performance in a typical case, we performed a thermal fluid simulation by setting the casing temperature as uniformly 60°C and the input coolant temperature

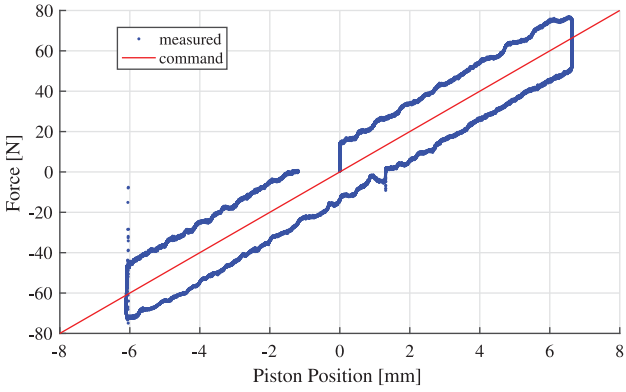

Figure 8. Relationship between the piston position and actuator force, when the actuator was under a low-gain position control and the piston was manually moved by hand. The straight line shows the desired force and the dot markers are the actual force. The force tracking error is due to the friction on the piston rod sealing, since the actuator's force measurement based on the pressure sensor cannot detect the friction. The RMS force tracking error was 12.1 N, which is 0.81% of the maximum output 1500 N.

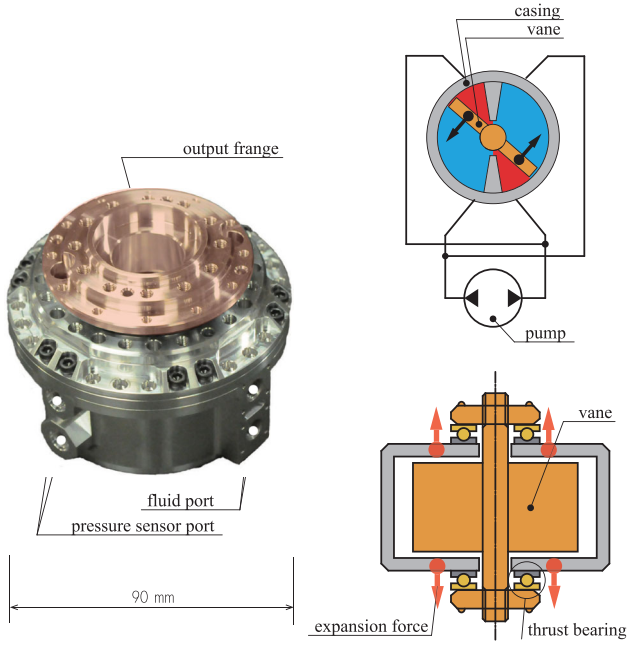

Figure 9. Picture and schematic of the developed double-vane motor. The expansion force due to the internal pressure, applied on the casing, is supported by a pair of thrust bearings held by the output shaft, therefore the strength of the pump casing can be reduced to save the total weight.

was 20°C with 4 cc/s flow rate. Its result is shown in the bottom right of Figure 10. The average temperature of the flowing out coolant was around 37°C, which means 290 W cooling capacity. While this value is higher than the rated power of the electric motor (200 W), it is not sufficient to constantly support the short term maximum actuator force. In the case that the robot simply keeps a standing posture, however, the consumption power of the whole body is around 500 W. Taking account that each leg has six DoF, we can assume that the cooling capacity is sufficiently high to maintain the system temperature when a proper interval is set between each heavy-duty tasks.

Table 2. Specification of the developed double vane motor.

Weight	780 g
Range of motion	120°
Maximum torque	60 N m
Maximum speed	290°/s

The maximum torque and speed shows the case with the pump described in Section 4.

To confirm the effect of the water cooling mechanism, we conducted a comparative experiment. The discharging port of the pump was closed and the inlet port was connected to an oil reservoir in the atmosphere. The pump was pressure controlled with a constant command pressure of 3.5 MPa. In one trial the coolant did not flow into the pump, while the other trial it did. The same pump was used for both of the trials to avoid the individual pump difference. The result is shown in Figure 11. In the graph, the red line represents the case without coolant flow and the blue line represents the case with the flow. The graph on the top shows the time transition of the measured pump pressure. The middle shows the time transition of the amount of the internal leakage. A clear difference can be seen from the graph. The amount of leakage in the case without cooling has a diverging behavior due to the positive feedback. With the water cooling, when 90 seconds after the beginning of the experiment, it suppressed 55% of the leakage compared with the case without cooling. The bottom graph shows the energy input to the pump from the motor. Since the discharging port of the pump is closed, all of the input energy is lost and converted to heat. The loss is the summation of the loss due to the friction and due to the internal leakage. This experiment was to clearly show the difference of the case with and without the cooling, therefore the target pressure was set as a high value. The 3.5 MPa pressure corresponds to 1000 N cylinder thrust force. In the practical use of the humanoid robot, it is rare to constantly require such force for more than 240 s, which is shown to be achieved in the graph. Table 3 summarizes the specification of the developed trochoid pump.

5. Cylinder bore maximization of a cluster actuator

As discussed in Section 2, larger pressure receiving surface can relax the gap and viscosity requirement. The key is how to maximize the usage of space in the limited outer size and overall weight. In this subsection, we show

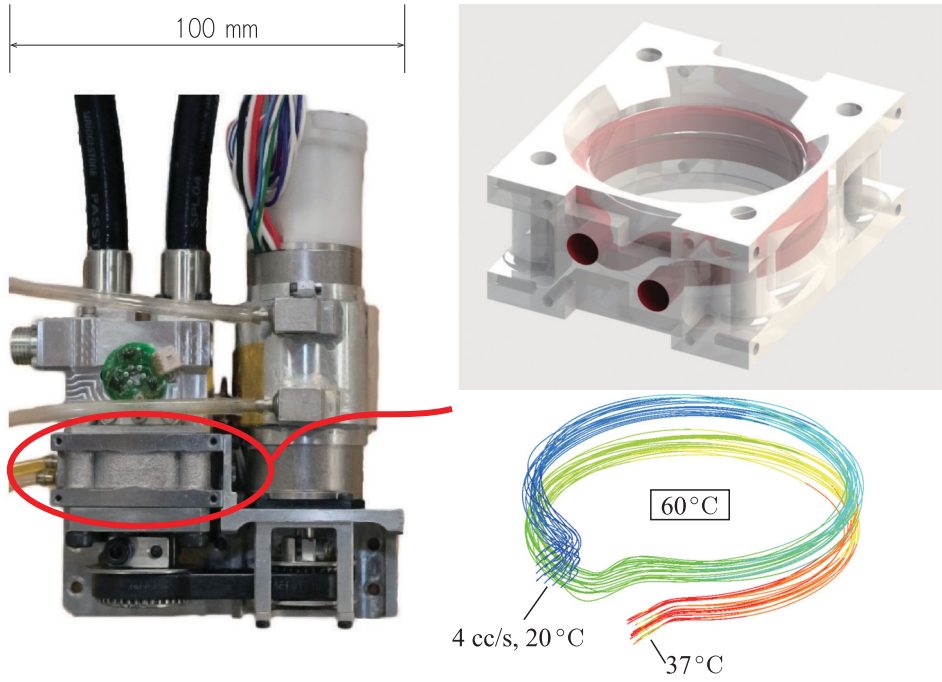

Figure 10. 3D printed integrated coolant flow channel in the pump casing. In a case when the casing is 60°C and the input coolant is 20°C with 4 cc/s flow rate, the cooling capacity is estimated to be 290 W from a thermal fluid simulation. This is higher than the 200 W rated power of the electric motor.

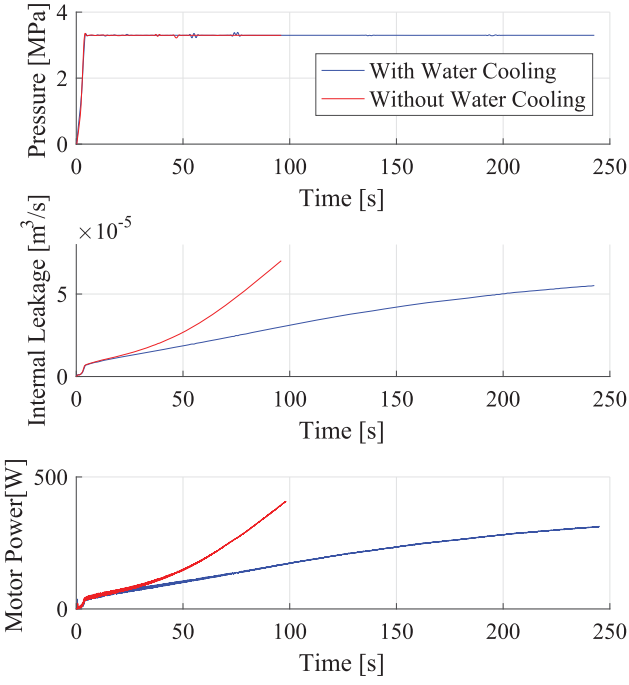

Figure 11. Time transition of the pump discharging pressure (top), amount of internal leakage (middle), and input power to the pump (bottom). The diverging line represents the case without water cooling and the converging line shows the case with water cooling. The discharging port of the pump is closed, the inlet port is connected to an oil reservoir in the atmosphere, and the pump is under a pressure feedback control. While in the case without the cooling, the internal leakage and the input power diverges. With the cooling, on the other hand, the values converge to a certain value.

Table 3. Specification of the developed trochoid pump.

Weight (including motor)	620 g
Motor power	200 W
Maximum discharge pressure	5.3 MPa
Displacement	418 mm^3/rev
Maximum discharge flow	57,000 mm^3/s

an enhancement of cylinder force by a design with high space usage efficiency. The target cylinder is the one for the hand [18], whose pump is already discussed in the previous Section 3.1. In its original design [20], multiple cylinders are integrated as a manifold, which is aluminum casted with a 3D printed plaster mold. While the distance between the pistons is 21 mm, the cylinder bore is 9 mm. Rather than the cylinder body itself, the main factor that restricts the cylinder bore is the termination part of the cylinder, such as the cone-shaped region to protect the piston seal in the assembling process, and the cap to close the cylinder end.

In the modified design, instead of the original merged cylinder body and separate termination part structure, we merge the termination parts (cylinder head) as a single piece, which closes multiple ends of the independent cylinder tubes. The fluid ports are also merged in the integrated cylinder head. The cylinder heads on both ends are connected with tie-rods. Since the manifold is a shared single piece, its high strength and stiffness allow free arrangement of the connecting rods according to the

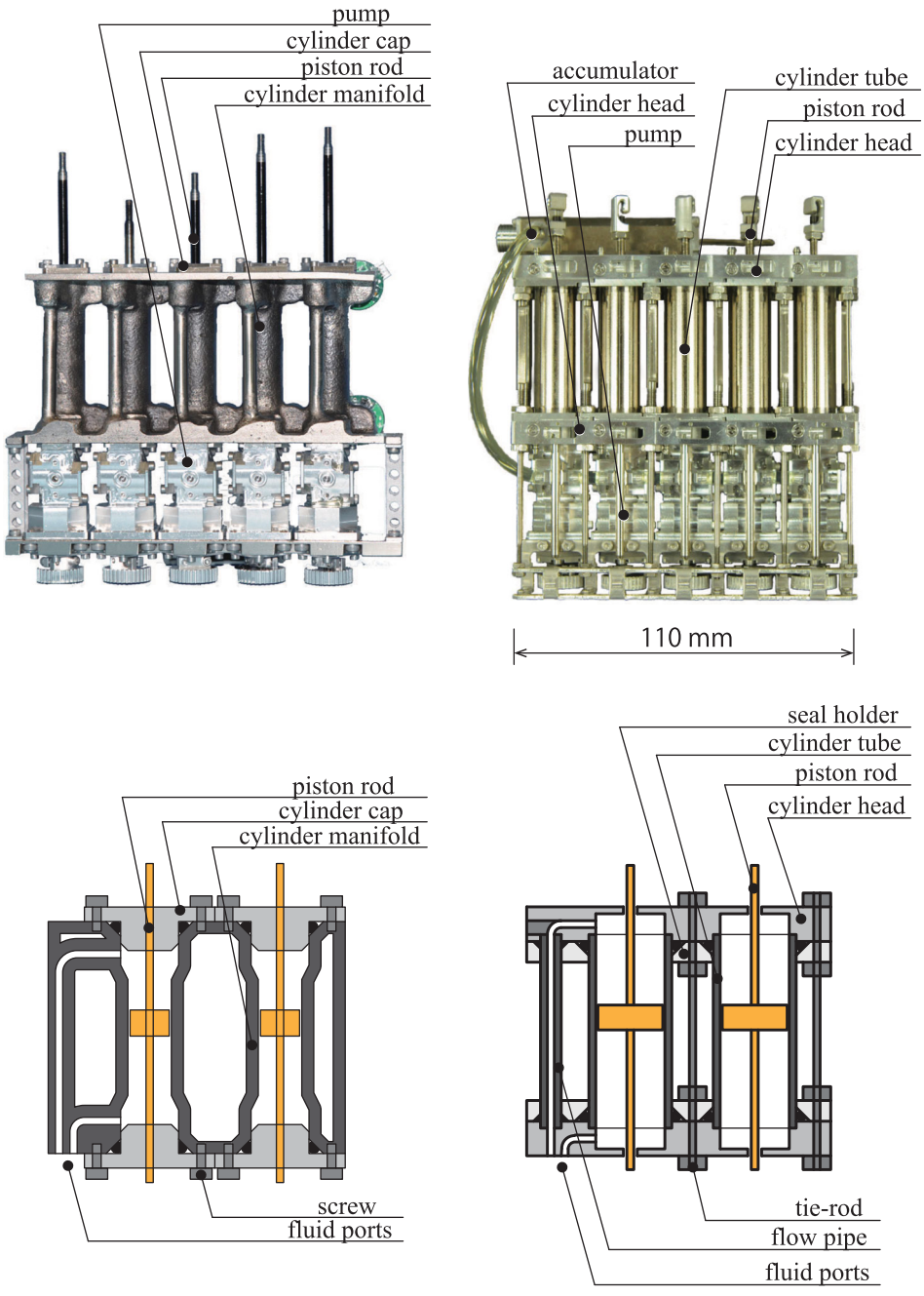

Figure 12. Schematic and picture of the developed cylinder cluster with casted cylinder manifold (left), and tie-rod cylinder cluster (right).

arrangement of cylinders. The components between each cylinder are now only O-rings to seal the gap between the cylinder head and cylinder tube. With this setup we can increase the cylinder bore from the previous 9 to 13 mm, keeping the same outer size of the cylinder cluster and the distance between each piston. This means 222% larger cylinder cross-section. (The total reduction ratio is almost the same, since the pump's displacement is also doubled, as explained in Section 3.1.) The approach also reduced 10% of the weight, from 224 to 200 g. This is the result of the optimization of the materials: the cylinder head is made of 7000 series aluminum alloy, the cylinder tube is made of 0.5 mm thickness chrome-molybdenum steel, while the tie-rods are titanium. Figure 12 shows the comparison of the original design and modified design.

Figure 13 shows a comparison of the force output of the initial actuator and the modified actuator. The pistons were fixed on the end of the cylinder. The command force was converted to the command pressure and the pumps were pressure controlled. The actuator forces are estimated from the pressure sensors. In both case 300 N command force, which was the initial requirement, was

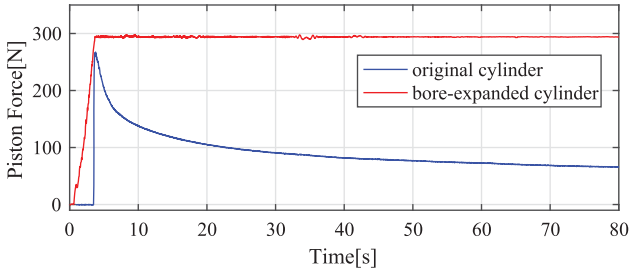

Figure 13. Comparison of piston force that the initial and modified actuator can output. Force is calculated through discharging pressure and piston diameters. The rising edges of the two graphs are different because smoother pressure reference was given to the modified pump. In both cases, the same electric motor and motor driver is used to drive the pump. The graph shows that with lower energy loss, the new actuator can exert 300 N force for a long time, which was impossible for the initial version.

Table 4. Specification of the developed 5-DoF cluster EHA for Hydra's hand.

Weight (including motors)	685 g
Motor power (each)	60 W
Cylinder bore	13 mm
Piston rod diameter	3 mm
Full stroke	40 mm
Maximum force	300 N
Maximum speed	60 mm/s

commanded to the actuator. In the case of the initial design, the force saturated from the beginning and it dropped with the time, since the poor energy efficiency results in a larger increase of the fluid temperature, which leads to less fluid viscosity and larger internal leakage. In the modified version, on the contrary, the actuator could successfully keep the force for more than 70 s. As a total, the specification of the cluster EHA for Hydra's hand is summarized in Table 4.

6. Conclusion

In this paper, we present our approach to enhance EHA's maximum force while keeping them small, lightweight and backdrivable, with which we create the hydrostatically driven humanoid robot 'Hydra'. The conclusion is as follows

(1) The best transmission efficiency of an EHA is realized on the balance of the loss due to viscous friction and the loss due to internal leakage, while miniaturization of the actuator moves the system to the internal leakage loss dominant side.
(2) To encounter the increase of internal leakage due to the reduced actuator size or weight, reduction of the internal gap, maintaining of the fluid viscosity, and full utilization of the space to enlarge the pressure receiving surface are effective.
(3) We presented the way to reduce the internal gap of the actuator on both of the pump and actuator side. On the pump side, we experimentally showed that with a modification on the bearing arrangement, bearing type and reinforcement of the pump casing, we can suppress the amount of internal leakage by more than 92%. On the actuator side, we first presented the design of a lightweight cylinder with no internal leakage. The developed cylinder had 600 g weight, 240 mm length, 20 mm cylinder bore, and 50 mm stroke. With its 6mm diameter piston rod, it converts the 5.3 MPa pump pressure to 1500 N piston force. It was experimentally showed that the cylinder has 12.1 N friction on the piston oil seal, which is as low as 0.81% of the maximum piston force. While cylinders are advantageous in the improvement of the force-to-weight ratio, to accommodate the situation that they are not available, we also presented a design of vane motor with special structure to attain both low internal leakage and lightweight. The developed vane motor had 780 g weight and 120° range of motion. The vane converts 5.3 MPa pump pressure to a 60 N m torque through the flange output.
(4) We proposed the direct pump casing water cooling approach to effectively suppress the positive feedback loop of that higher fluid temperature results in lower viscosity, then lower efficiency and the even more energy loss. We experimentally showed that the water cooling could suppress the internal leakage by 55%.
(5) We showed the way to maximally utilize the space to increase the effective pressure receiving surface of a cluster actuator. It was experimentally shown that the modification of an EHA, which is to double both the piston surface and the pump displacement, drastically improved the performance. Combined with the higher stiffness pump, the modified actuator could output 300 N force for more than 70 s, which was not possible for even a short time in the initial design.

Note

1. Here we treat the overall reduction ratio is given, therefore the cylinder surface is automatically decided according to *r*.

Disclosure statement

No potential conflict of interest was reported by the authors.

Funding

This work was supported by New Energy and Industrial Technology Development Organization (NEDO). The International R&D and Demonstration Project on Robotic Field /Research and Development of Disaster-Response Robot Open Platform (FY2014-FY2015).

Notes on contributors

Tianyi Ko received his BEng, MEng, and PhD degrees in Mechano-Informatics from the University of Tokyo, Japan, in 2013, 2015, and 2018, respectively. He is the recipient of the IEEE Robotics and Automation Society Japan Joint Chapter Young Award in 2017, and Jc-IFToMM Young Investigator Fund Best Paper Award in 2018. He is currently a researcher in Preferred Networks, Inc.

Hiroshi Kaminaga received PhD from The University of Tokyo in 2009. He was an Assistant Professor of The University of Tokyo from 2009 to 2017. He is currently a Senior Researcher at National Institute of Advanced Industrial Science and Technology (AIST). His research interests are the mechatronic design and control of force sensitive actuators, and its application to robot systems including humanoid robots. e is a member of IEEE, The Robotics Society of Japan (RSJ), and The Society of Instrument and Control Engineers (SICE).

Yoshihiko Nakamura received PhD from the Kyoto University in 1985. He was an Assistant Professor of Kyoto University and then Assistant and Associate Professor of University of California, Santa Barbara, before he joined the University of Tokyo in 1991. He is currently a Professor at Department of Mechano-Informatics. Humanoid robotics, cognitive robotics, neuro musculoskeletal human model, and their computational algorithms are his current fields of research. Dr. Nakamura served as a President of IFToMM (2011–2015). He is a Fellow of Japan Society of Mechanical Engineers, Fellow of Robotics Society of Japan, Fellow of IEEE, and Fellow of World Academy of Arts and Science. Dr. Nakamura is a Foreign Member of Academy of Engineering Science of Serbia, and TUM Distinguished Affiliated Professor of Technische Universitt Mnchen.

References

[1] Asada H, Kanade T. Design concept of direct-drive manipulators using rare-earth DC torque motors. Proceedings of the International Joint Conference on Artificial Intelligence; 1981. p. 775–778.
[2] Wensing PM, Wang A, Seok S, et al. Proprioceptive actuator design in the MIT cheetah: impact mitigation and high-bandwidth physical interaction for dynamic legged robots. IEEE Trans Robot. 2017;33(3):509–522.
[3] Hill A. The heat of shortening and the dynamic constants of muscle. Proc R Soc London B Biol Sci. 1938;126(843):136–195.
[4] Hyodo K, Kobayashi H. A study on tendon controlled wrist mechanism with nonlinear spring tensioner. J Robot Soc Jpn. 1993;11(8):1244–1251.
[5] Pratt G, Williamson M. Series elastic actuators. Proceedings of IEEE/RSJ International Conference on Intelligent Robots and Systems; 1995. p. 399–406.
[6] Tsagarakis NG, Caldwell DG, Negrello F, et al. Walkman: a high-performance humanoid platform for realistic environments. J Field Robot. 2017;34(7):1225–1259.
[7] Stentz A, Herman H, Kelly A, et al. Chimp, the cmu highly intelligent mobile platform. J Field Robot. 2015;32(2):209–228.
[8] Knabe C, Seminatore J, Webb J, et al. Design of a series elastic humanoid for the DARPA robotics challenge. Proceedings of IEEE-RAS International Conference on Humanoid Robots; 2015. p. 738–743.
[9] Grebenstein M, Albu-Schäffer A, Bahls T, et al. The DLR hand arm system. Proceedings of IEEE International Conference on Robotics and Automation; 2011. p. 3175–3182.
[10] Hunter IW, Hollerbach JM, Ballantyne J. A comparative analysis of actuator technologies for robotics. Robot Rev. 1991;2:299–342.
[11] Caldwell DG, Medrano-Cerda GA, Bowler CJ. Investigation of bipedal robot locomotion using pneumatic muscle actuators. Proceedings of IEEE International Conference on Robotics and Automation; 1997. p. 799–804.
[12] Verrelst B, Vanderborght B, Vermeulen J, et al. Control architecture for the pneumatically actuated dynamic walking biped lucy. Mechatronics. 2005;15(6):703–729.
[13] Niiyama R, Nishikawa S, Kuniyoshi Y. Athlete robot with applied human muscle activation patterns for bipedal running. IEEE-RAS International Conference on Humanoid Robots; 2010. p. 498–503.
[14] Kaminaga H, Yamamoto T, Ono J, et al. Backdrivable miniature hydrostatic transmission for actuation of anthropomorphic robot hands. Proceedings of IEEE-RAS International Conference on Humanoid Robots; 2007. p. 36–41.
[15] Alfayad S, Ouezdou FB, Namoun F, et al. High performance integrated electro-hydraulic actuator for robotics. Part II: theoretical modelling, simulation, control & comparison with real measurements. Sens Actuators A: Phys. 2011;169(1):124–132.
[16] Kaminaga H, Ko T, Masumura R, et al. Mechanism and control of whole-body electro-hydrostatic actuator driven humanoid robot hydra. International Symposium on Experimental Robotics. Springer; 2016. p. 656–665.
[17] Kaminaga H, Amari T, Katayama Y, et al. Backdrivability analysis of electro-hydrostatic actuator and series dissipative actuation model. Proceedings of IEEE International Conference on Robotics and Automation; 2010. p. 4204–4211.
[18] Ko T, Kaminaga H, Nakamura Y. Underactuated four-fingered hand with five electro hydrostatic actuators in cluster. Proceedings of IEEE International Conference on Robotics and Automation; 2017. p. 620–625.
[19] Nsk micro precision co., Ltd. Thrust angular contact bearing corxy. Available from: http://wwwnskmicrocojp/english/products/products01_09html.
[20] Kang T, Kaminaga H, Nakamura Y. A robot hand driven by hydraulic cluster actuators. Proceedings of IEEE-RAS International Conference on Humanoid Robots; 2014. p. 39–44.